Springer

Journal of Mechanical Science and Technology 23 (2009) 1773~1778

Journal of Mechanical Science and Technology

www.springerlink.com/content/1738-494x
DOI 10.1007/s12206-009-0602-2

Strengths of horseshoe vortices around a circular cylinder with an upstream cavity †

K. J. Kang[1], T. Kim[2] and S. J. Song[3,*]

[1]*Intelligent System Research Division, Korea Institute of Science and Technology, Seoul, Korea*
[2]*MOE Key Laboratory for Strength and Vibration, Xi'an Jiaotong University, Xi'an, P.R. China*
[3]*School of Mechanical and Aerospace Engineering, Seoul National University, Seoul, Korea*

(Manuscript Received March 20, 2009; Revised March 25, 2009; Accepted March 27, 2009)

Abstract

Horseshoe vortices are formed at the junction of an object immersed in fluid-flow and endwall plate as a result of three-dimensional boundary layer separation. This study presents the variation of the strengths of such horseshoe vortices around a circular cylinder with a cavity (slot) placed upstream. Through the cavity, no mass flow addition (blowing) or reduction (suction) is applied. With the upstream cavity, adverse pressure gradient is weakened upstream of the cavity whereas it is strengthened downstream of the cavity. Furthermore, a single vortex system is found to form immediately upstream of the cylinder instead of a typical two vortex (primary and secondary vortices) system observed in the absence of the upstream cavity. The strength of the primary vortex is weakened due to the fluid stream engulfed in to the upstream cavity, resulting in diffusion of the mainstream. Consequently, the circulation of the primary vortex is weakened.

Keywords: Horseshoe vortices; Upstream cavity; Vorticity

1. Introduction

The boundary layer approaching an obstacle protruding from an endwall experiences an adverse pressure gradient in the direction of the mainstream. Subsequently, the incoming boundary layer forms a classical vortical structure, the so-called "horseshoe vortex" around the junction of the obstacle and endwall. In accordance with Kelvin's circulation theorem, the boundary layer vorticity cannot be destroyed. Instead, it is convected around each side of the obstacle to form two legs of the horseshoe vortex.

Due to the practical importance associated with the horseshoe vortex in terms of secondary loss generation and local heat transfer, a considerable amount of research on horseshoe vortex has been conducted [1-6]. It has been numerically and experimentally explored that the horseshoe vortex system could consist of multiple pairs of counter-rotating vortices which undergo cyclic-periodic events at high Reynolds numbers [4]. The exact number of vortex pairs depends on flow conditions according to Visbal [6].

Some topological models of the horseshoe vortex system in the plane of symmetry have been proposed [3, 6-8]. Khan and Ahmed [3] compared previously reported topological models and proposed that the topology varies with flow regime from a single to a three-vortex pair (i.e., three pairs of counter-rotating vortices) system.

In turbomachinery, such juncture flow is observed when mainstream passes through compressor/turbine's blades. For example, a stator can be shrouded, configuring an upstream cavity to the stator blades (Fig. 1). There is the addition of mass flow through the upstream cavity for compressors whilst the reduction of mass flow exists for turbines due to the corre-

† This paper was presented at the 7th JSME-KSME Thermal and Fluids Engineering Conference, Sapporo, Japan, October 2008.

*Corresponding author. Tel.: +82 32 872 309682 2 880 1667, Fax.: +82 32 868 171682 2 883 0179
E-mail address: kykim@inha.ac.krsjsong@snu.ac.kr

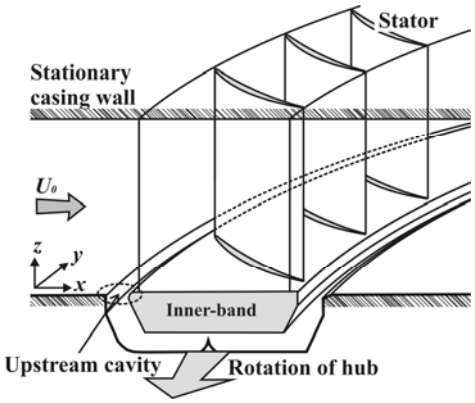

Fig. 1. Schematic of shrouded stator hub in an axial compressor.

sponding pressure gradient in the direction of the mainstream. A significant part of the overall loss and performance degradation of such turbomachines has been attributed to the formation and variation of the horseshoe vortices in the junction between the stators and hub. To reduce these negative effects of the horseshoe vortices, numerous studies have focused on this topic.

Devenport et al. [9] examined the effects of a constant-radius circular concave fillet near the blade vertex, making the blade shape blunt and delaying the leading edge separation. In their subsequent work [10], a leading-edge fillet was found to reduce adverse pressure gradients and retard separation. Another popular method is to actively control the upstream boundary layer by either suction or blowing. Philips et al. [11] used a suction slot and found disappearance of the large-scale horseshoe vortex. Johnson et al. [12] also examined the role of blowing through the upstream hole. They found that, with increasing blowing rate, the formation of the horseshoe vortex was delayed.

This paper examines the weakening of the horseshoe vortices around a single cylinder due to an upstream cavity at Re_D=2.0×10^4. Velocity field near the junction in the symmetry plane and endwall surface flow patterns has been experimentally measured with no mass flow addition (blowing) or reduction (suction) through the upstream cavity.

2. Experimental details

2.1 Wind-tunnel facility and cylinder models

An open-type wind-tunnel has been used for endwall surface flow visualization using oil-dye tech-

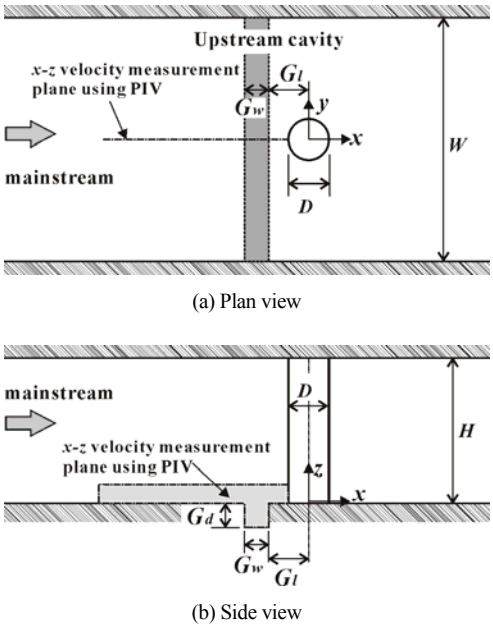

Fig. 2. Schematic of test setup showing a single cylinder placed in a rectangular channel with upstream cavity (slot).

nique and flow field visualization using particle image velocimetry (PIV). A centrifugal fan blows air that passes through a settling chamber, screens, and honeycomb section. A schematic of the test section with an upright cylinder mounted on a flat endwall is illustrated in Fig. 2. The size of a rectangular test section is 0.18 m (H) × 0.30 m (W). A single circular cylinder with a diameter (D) of 0.05 m has been fabricated for testing. A 0.03 m (G_w) × 0.03 m (G_D) × 0.04 m (G_l) upstream cavity covers a longitudinal range from -0.8D to -1.4D upstream measured from the center of the cylinder axis as illustrated in Fig. 2(b).

2.2 Oil-dye surface flow visualization, pressure and velocity field measurements

Endwall surface flow pattern has been visualized using an oil-dye mixture technique in the wind-tunnel. Florescent powder is mixed with a light diesel fuel, and the mixture is then applied to the cylinder surface. Before the application of the mixture, the surface is painted in black to enhance reflectivity when using ultraviolet light to illuminate the surface flow pattern.

To monitor the mainstream velocity, a Pitot tube is positioned at 4.4D upstream from the cylinder axis. In total, 10 static pressure tappings are distributed on the endwall along the direction of mainstream, coinciding

with the plane of symmetry i.e., the x-axis. The pressure tappings and stagnation pressure probes are connected to a differential pressure transducer (Scanivalve Inc.) which sends data via a RS232 cable to a data acquisition personal computer.

To obtain flow field around the junction of the cylinder and endwall, particle image velocimetry (PIV) - composed of a double pulsed Nd: YAG laser generator, a CCD camera, and a seed particle generator - has been used. A 1-mm thick laser sheet has been created by an optical system and aligned with the cylinder axis (y=0) for the x-z plane flow measurement. Prior to the measurement, the flat plate is painted in black to minimize reflection. Based on the flow velocity and the focal length of a 12-bit CCD camera to the measurement plane, the time interval (Δt) of each pair of the captured images (1375×1024 pixels) has been set to be 80 μs. The instantaneous velocity fields are then obtained using a cross-correlation analysis with an interrogation window of 16×16 pixels and a 50% overlap providing vector-to vector spacing. In total, 1,000 instantaneous flow images have been captured with a sampling frequency of 15 Hz followed by ensemble averaging.

2.3 Data reduction parameters and measurement uncertainty

Local static pressure on the endwall is evaluated using a nondimensional parameter, wall pressure coefficient (C_p) defined as:

$$C_p = \frac{p(x/D) - p_{amb}}{\rho U_0^2 / 2} \tag{1}$$

where $p(x/D)$ and p_{amb} are static upstream pressure and reference ambient pressure, respectively.

The uncertainty associated with the wall pressure coefficient is estimated following a method reported by Coleman and Steele [13] (based on 20:1 odds) and found to be within 1.1%. Note that only random errors are considered here. It is assumed that the bias (systematic) errors could be minimized by careful calibrations.

For error analysis in PIV measurements, it is assumed that the vortical flow motion around the cylinder junction is well traced by the tracer particles and the time interval of each pair of pulse laser sheets has been set accurately. The latter implies that errors in the local velocity components in the x-z plane mainly stem from the displacement of tracer particles. According to Wernet [14], the displacement estimate σ_D is primarily determined by the ratio of the correlation peak width d_r (unit: pixel) to the average particle displacement D_P (unit: pixel) across the interrogation window (sub-region), expressed as:

$$\sigma_D = d_r / D_p \tag{2}$$

where

$$D_p = 1000(\Delta t V_{avg}) / B \tag{3}$$

Here, V_{avg} is the actual average velocity of seed particles in the flow field. Also, B is the ratio of the actual particle displacement (unit: mm) to the corresponding total number of pixels the tracer particles travel (unit: pixel). Following a method reported by Wernet [14], uncertainty of the measured x-z velocity components in this study using PIV is estimated to be within 2.5%.

3. Results and discussions

3.1 Foot-prints of horseshoe vortices on endwall surface

The mean characteristics of endwall surface flows - the footprints of horseshoe vortices formed around a single cylinder- are shown in Fig. 3(a), demonstrating a well-known horseshoe vortex system at Re_D = 2.0×10^4. Since only the time averaged behavior of the horseshoe vortex system is captured, the flow pattern is symmetric with respect to the x-axis.

For the interpretation of such flow images, some topological models have been proposed [3, 7, 8]. A common feature suggested is the saddle point (S) referring to a point through which two particular streamlines pass. Each line acts as a barrier in the field of limiting streamlines so that one set of streamlines cannot cross another set of streamlines. A saddle point, or the position of the primary separation (λ_s), is located at approximately at 1.3D upstream from the cylinder axis (or 0.8D from the leading edge). This value lies within range ($0.8D < \lambda_s < 1.5D$) collected by Ballio et al. [1]. In this photograph, the separation lines are indicated by brighter lines as a result of accumulated dye particles. On the lower half of the flow image, attachment (dotted) and separation (solid) lines are sketched over the image.

With the presence of the upstream cavity covering a range of $-1.4 \le x/D \le -0.8$, the pattern of the horse shoe vortex formation is expected to differ. Fig. 3(b)

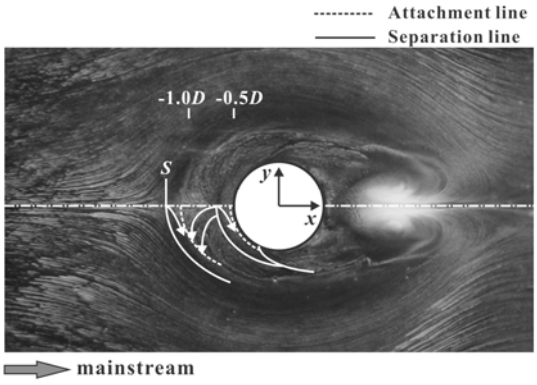

(a) Without upstream cavity (reference)

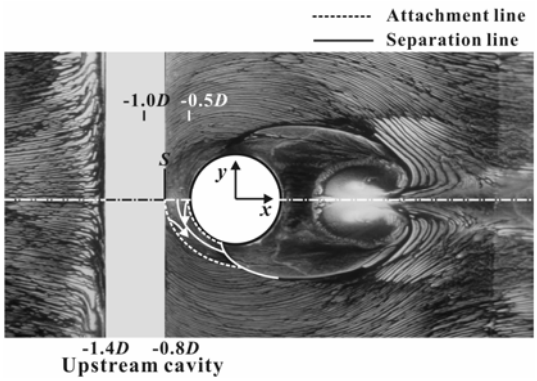

(b) With upstream cavity

Fig. 3. Endwall surface flow images around a cylinder.

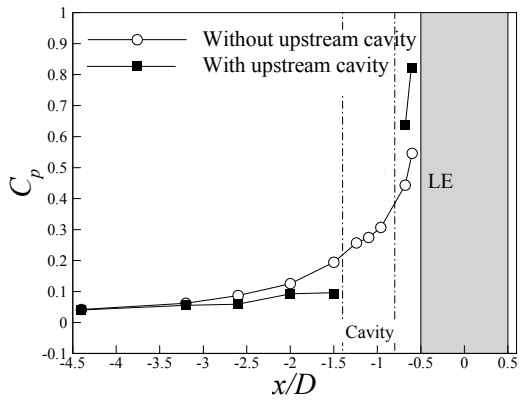

Fig. 4. Longitudinal pressure gradient along the symmetry line on the upstream section.

exhibits that only a single vortex near the leading edge of the cylinder is strong enough to be marked. Also, the outermost line appears to be the line of attachment unlike the line of separation which was observed there for the reference case. This flow feature may indicate that the flow separated from the upstream edge of the cavity reattaches in this region.

3.2 Adverse pressure gradient

The approaching boundary layers experience an adverse pressure gradient due to the cylinder. To evaluate the adverse pressure gradient upstream of the cylinder leading edge, the static pressures at selected longitudinal locations in the plane of symmetry has been measured, and results are plotted in Fig. 4.

The pressure data without upstream cavity in Fig. 4 show that C_p monotonically and significantly increases up to the leading edge of the cylinder. This pressure rise (or adverse pressure gradient) is mainly due to the stagnation of the mainstream on the leading edge of the cylinder mounted normal to the endwall. With the upstream cavity, the increase in C_p before the upstream cavity is gradual compared to that without the upstream cavity. No data points are measured in the cavity. In the region between the upstream cavity and the leading edge of the cylinder, C_p data show higher values and gradient than those for without the cavity. This feature may be associated with the flow that is separated from the upstream edge of the cavity diffusing and reattaching in this region.

3.3 Vortical flow structures in the plane of symmetry

To identify the dominant vortical flow structures responsible for the observed surface flow features especially at the junction of the cylinder and endwall including the upstream cavity, velocity fields in the plane of symmetry have been obtained using PIV at $Re_D = 2.0\times10^4$.

For the reference case (without the upstream cavity), a classical two-vortex system (i.e., two pairs of counter-rotating vortices) around the cylinder is visible in Fig. 5(a). This result is consistent with the endwall flow observation. A primary vortex (V_1) rotating clockwise is formed immediately upstream of the cylinder leading edge followed by a second vortex (V_2) also rotating clock-wise. There must be counter-rotating vortices to satisfy the topology rule [3, 8, 15], but they lie very close to the surface and are not clearly visible in Fig. 5(a). The cores of the two vortices are located approximately at x/D = -0.70 and -0.95, respectively, from the cylinder axis. Although these locations are not representative of steady state features because their locations vary in time, it can be, at least, the evidence of the two vortex system formed in this study. According to a survey of time-averaged

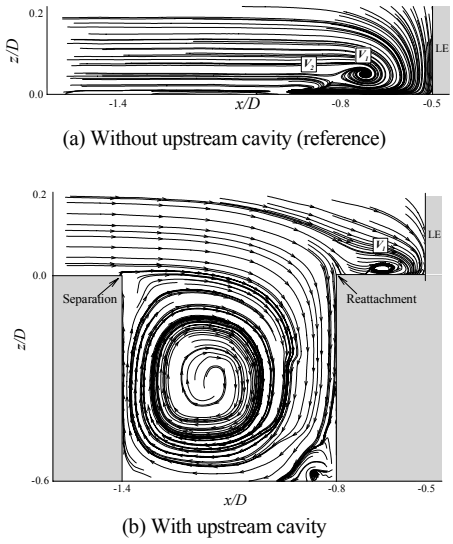

(a) Without upstream cavity (reference)

(b) With upstream cavity

Fig. 5. Horseshoe vortex system measured in the plane of symmetry upstream using PIV.

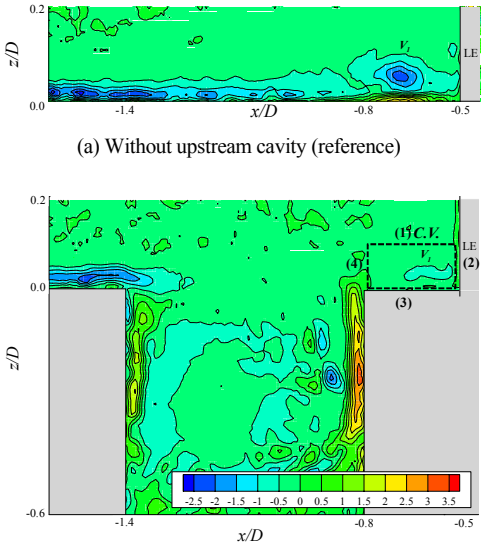

(a) Without upstream cavity (reference)

(b) With upstream cavity

Fig. 6. Vorticity contours in the plane of symmetry.

characteristics of laminar and turbulent horseshoe vortices [1], the longitudinal position (λ_o) of the primary vortex formed around the cylinder is located in the range of $0.65D < \lambda_o < 0.8D$, showing good agreement with that measured in the present study ($\lambda_o \sim 0.7D$).

With the upstream cavity, only a single vortex is captured as also observed from the endwall surface flow image (Fig. 3(b)). The longitudinal location of the primary vortex (V_1) seems to move slightly closer to the leading edge of the cylinder ($\lambda_s = 0.65D$ from $\lambda_s = 0.7D$ for the reference case). The flow separated from the upstream cavity is engulfed into the cavity, forming a large vortical flow in the cavity as clearly seen in Fig. 5(b). Separated by "the dividing streamline," the outer flow reattaches between the upstream cavity and cylinder leading edge.

In addition to the axial location of the primary vortex, the circulation associated with the vortex is influenced by the upstream cavity. To compare the variation of the vortex strength (i.e., circulation) due to the upstream cavity, a control volume containing the primary vortex is selected as shown in Fig. 6(b). Circulation is calculated by taking the line integral along the dashed contour A as:

$$\Gamma = \iint_A \omega dA = \int_{(1)} v_x dx + \int_{(2)} v_z dz + \int_{(3)} v_x dx + \int_{(4)} v_z dz \qquad (4)$$

where ω is the vorticity of the primary vortex (V_1) defined as:

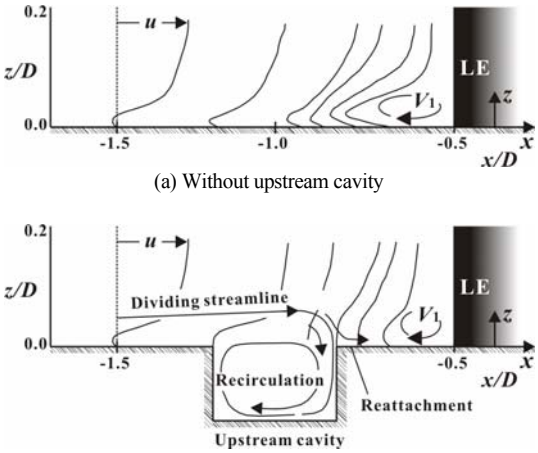

(a) Without upstream cavity

(b) With upstream cavity

Fig. 7. Evolution of the streamwise velocity field in the plane of symmetry (inferred from PIV data).

$$\omega = \frac{\partial v_z}{\partial x} - \frac{\partial v_x}{\partial z} \qquad (5)$$

Here, v_x and v_z are, respectively, the x- and z- velocity components extracted from the PIV data. Vorticity contours calculated from the velocity field in Fig. 5 are depicted in Fig. 6, and they indicate a 78 % reduction of the vorticity of the primary vortex (V_1) due to the presence of the upstream cavity.

Fig. 7 illustrates the streamwise variation of the velocity profile in the plane of symmetry for both cases,

inferred from the PIV data. There exist two fluid streams divided by the dividing streamline. The fluid stream below the dividing streamline is engulfed into the upstream cavity. Therefore, the fluid stream above the dividing streamline experiences diffusion, leading to the decrease in the streamwise velocity. Consequently, the circulation of the primary vortex is weakened.

4. Conclusions

The strengths of horseshoe vortices formed around a circular cylinder have been experimentally examined, including its variation due to the presence of an upstream cavity at $Re_D = 2.0\times10^4$. No mass addition (or reduction) has been applied through the upstream cavity. The juncture flow features associated with the upstream cavity are summarized as follows.

1) For the cylinder without an upstream cavity, a two-vortex system has been found to form. In this regard, the endwall surface images and detailed flow field data from PIV in the plane of symmetry are consistent.

2) The outermost line of the horseshoe vortices, which is the line of separation without a cavity, becomes the line of attachment of a single vortex in the presence of an upstream cavity.

3) With upstream cavity, the adverse pressure gradient is reduced upstream of the cavity but slightly strengthened in the region between the cavity and the leading edge of the cylinder.

4) The upstream cavity causes diffusion of the fluid stream above the dividing streamline. Consequently, the circulation of the primary vortex is weakened.

References

[1] F. Ballio, C. Bettoni and S. Franzetti, A survey of time-averaged characteristics of laminar and turbulent horseshoe vortices, J. Fluids Engineering 120 (1998) 233-242.

[2] C. J. Baker, The turbulent horseshoe vortex, J. Wind Engineering and Industrial Aerodynamics 6 (1980).

[3] M. J. Khan and A. Ahmed, Topological model of flow regimes in the plane of symmetry of a surface-mounted obstacle, Phys. Fluids 17 (2005) 045101.

[4] C. V. Seal, C. R. Smith and D. Rockwell, Dynamics of the vorticity distribution in endwall junctions, AIAA J. 35 (1997) 1041-1047.

[5] R. L. Simpson, Junction flows, Annu. Rev. Fluid Mech. 33 (2001) 415-443.

[6] M. R. Visbal, Structure of laminar juncture flows, AIAA J. 29 (1991) 1273-1282.

[7] J. C. R. Hunt, C. J. Abell, J. A. Petetka and H. Woo, Kinematical studies of the flows around free or surface-mounted obstacles; applying topology to flow visualization, J. Fluid Mech. 86 (1978)179-200.

[8] M. Tobak and D. J. Peake, Topology of two-dimensional and three-dimensional separated flows, AIAA 12th Fluid and Plasma Dynamics Conference, AIAA paper (1979) 79-1480.

[9] W. J. Devenport, M. B. Dewitz, N. K. Agarwal, R. L. Simpson, K. Podder, Effects of a fillet on the flow past a wing body junction, AIAA Paper (1989) 89-0986.

[10] W. J. Devenport, R. L. Simpson, M. B. Dewitz, N. K. Agarwal, Effects of a leading-edge fillets on the flow past an appendage-body junction, AIAA Paper (1991) 91-0252.

[11] D. B. Philips, J. M. Cimbala, A. L. Treaster, Suppression of the wing-body junction vortex by body surface suction, J. Aircraft 29 (1991) 118-122.

[12] M. J. Johnson, K. Ravindra and R. Anres, Comparative study of the elimination of the wing fuselage junction vortex by boundary layer suction and blowing, AIAA Paper (1994) 94-0293.

[13] H. W. Coleman and W. G. Steele, Experimentation and uncertainty analysis for engineers, 2nd Edition, John Wiley and Sons, New York (1999).

[14] M. P. Wernet, Application of DPIV to study both steady state and transient turbomachinery flows, Optics & Laser Technology 32 (2000) 497-525.

[15] A. E. Perry and M. S. Chong, Interpretation of flow visualization, Flow visualization editted by A, J. Smits and T. T. Lim, Imperial College Press 2003.

Seung Jin Song has received his undergraduate and graduate degrees from Duke University and MIT, respectively. He has taught in the Department of Aerospace Engineering at Inha University from 1995 to 1999. Since 1999, he has been teaching in the School of Aerospace Engineering at Seoul National University. His research interests include turbomachinery, propulsion, and fluid engineering.